Published in final edited form as:
Hepatology. 2012 February ; 55(2): 609–621. doi:10.1002/hep.24713.

A mouse model of accelerated liver aging due to a defect in DNA repair

Siobhán Q. Gregg[1,2], **Verónica Gutiérrez**[1,2], **Andria Rasile Robinson**[2,3], **Tyler Woodell**[2], **Atsunori Nakao**[4], **Mark A. Ross**[5], **George K. Michalopoulos**[6], **Lora Rigatti**[6], **Carrie E. Rothermel**[5], **Irene Kamileri**[7,8], **George Garinis**[7,8], **Donna Beer Stolz**[5], and **Laura J. Niedernhofer**[1,2,*]

[1]Department of Microbiology and Molecular Genetics, University of Pittsburgh School of Medicine, 523 Bridgeside Point II, 450 Technology Drive, Pittsburgh, PA 15219 USA

[2]University of Pittsburgh Cancer Institute, 5117 Centre Ave, Hillman Cancer Center, 2.6, Pittsburgh, PA 15213 USA

[3]Department of Human Genetics, University of Pittsburgh School of Public Health, 130 DeSoto Street, Pittsburgh, PA 15261 USA

[4]Department of Surgery, Thomas E. Starzl Transplantation Institute, University of Pittsburgh, Pittsburgh PA 15213 USA

[5]Department of Cell Biology and Physiology, University of Pittsburgh School of Medicine, S362 Biomedical Science Towers, 3500 Terrace Street, Pittsburgh, PA 15261 USA

[6]Department of Pathology, University of Pittsburgh School of Medicine, S-417 Biomedical Science Towers, 200 Lothrop Street, Pittsburgh, PA 15216 USA

[7]Institute of Molecular Biology and Biotechnology, Foundation for Research and Technology-Hellas, Nikolaou Plastira 100, 70013, Heraklion, Crete, Greece

[8]Department of Biology, University of Crete, Vassilika Vouton, GR71409, Heraklion, Crete, Greece

Abstract

The liver changes with age leading to an impaired ability to respond to hepatic insults and increased incidence of liver disease in the elderly. Therefore, there is critical need for rapid model systems to study aging-related liver changes. One potential opportunity is murine models of human progerias, or diseases of accelerated aging. *Ercc1*$^{-/\Delta}$ mice model a rare human progeroid syndrome caused by inherited defects in DNA repair. To determine if hepatic changes that occur with normal aging occur prematurely in *Ercc1*$^{-/\Delta}$ mice, we systematically compared liver from 5 month-old, progeroid *Ercc1*$^{-/\Delta}$ mice to old (24–36 month) wild-type (WT) mice. Both displayed areas of necrosis, foci of hepatocellular degeneration and acute inflammation. Loss of hepatic architecture, fibrosis, steatosis, pseudocapillarization, and anisokaryosis were more dramatic in *Ercc1*$^{-/\Delta}$ mice than in old WT mice. Liver enzymes were significantly elevated in serum of *Ercc1*$^{-/\Delta}$ mice and old WT mice, while albumin was reduced, demonstrating liver damage and dysfunction. The regenerative capacity of *Ercc1*$^{-/\Delta}$ liver following partial hepatectomy was significantly reduced. There was evidence of increased oxidative damage in *Ercc1*$^{-/\Delta}$ and old WT liver, including lipofuscin, lipid hydroperoxides and acrolein as well as increased hepatocellular senescence. There was a highly significant correlation in genome-wide transcriptional changes

*Corresponding author: Dr. Laura J. Niedernhofer, MD, PhD, 5117 Centre Ave, Hillman Cancer Center, Office 2.6, Pittsburgh, PA 15213 USA, Telephone: (412) 623-7763, Fax: (412) 623-7761, niedernhoferl@upmc.edu.

between old WT and 16 but not 5 week-old *Ercc1*$^{-/\Delta}$ mice emphasizing that the *Ercc1*$^{-/\Delta}$ mice acquire an aging profile in early adulthood.

Conclusion—There are strong functional, regulatory and histopathological parallels between accelerated aging driven by a DNA repair defect and normal aging. This supports a role for DNA damage in driving aging and validates a murine model for rapidly testing hypotheses about causes and treatment for aging-related hepatic changes.

Keywords

DNA repair; DNA damage; progeria; hepatic fibrosis; mouse model

INTRODUCTION

Aging is characterized by the progressive loss of homeostatic reserve in all tissues leading to a decreased ability to respond to stress, functional decline and dramatically increased risk of morbidity and mortality(1). Chronic liver disease and cirrhosis are the twelfth leading cause of death in the United States, with 25,192 (1.1%) deaths each year(2). Mortality due to liver disease is not limited to the United States, as the World Health Organization (WHO) estimates that 20 million individuals have cirrhosis and/or liver cancer worldwide, and that 1–2 million die annually as a result of liver failure. Many liver diseases are more prevalent in the elderly, including alcohol-induced cirrhosis, viral hepatitis-induced cirrhosis, diabetic-associated chronic liver disease, hepatocellular carcinoma and biliary cirrhosis(3, 4), illustrating that aged liver is less able to cope with a variety of stressors.

Although there are no definitive biomarkers of aged liver, there are several hallmark structural changes. The volume of the liver decreases with age(5). This decrease is gender-specific, with an average decrease of 6.5% in males and 14.3% in females(6). Hepatocytes are quiescent cells, until stimulated to proliferate following injury or surgical resection(7). The capacity for hepatocyte regeneration following partial hepatectomy decreases with age(8). During the aging process, the nuclear size and shape of hepatocytes becomes altered(9). Nuclear invaginations and larger nuclei are commonly associated with age in liver samples(10). Nuclear polyploidy of hepatocytes increases with age, rising from 7–10% in young mice to approximately 30% in old mice(9). Finally, lipofuscin, insoluble oxidized proteins, accumulates in the cytoplasm of hepatocytes(11, 12).

Liver sinusoidal endothelial cells (LSEC) line the hepatic microvasculature, express little to no basement membrane, and exhibit numerous fenestrations necessary for filtering lipopoteins from the portal blood supply. A reduction in the number of these pores combined with the thickening of the endothelium, called pseudocapillarization, is commonly seen in aged livers(13), as is non-alcoholic fatty liver disease or steatosis(14). The underlying cause for fatty liver disease is not known, but some possibilities include diabetes mellitus, oxidative stress, mitochondrial dysfunction and metabolic and hormonal imbalances(15). All of these age-related liver changes in humans are recapitulated in the mouse(16–20).

Aging research is challenging because of the incredible variability in humans. Mice offer an attractive alternative because genetic and environmental variables can be controlled. Nevertheless, the time and expense required to generate and maintain mice >3 years of age is daunting. One approach to overcome this is to use mouse models of accelerated aging, or human progerias. Werner syndrome, Cockayne syndrome, XFE progeroid syndrome and trichothiodystrophy are examples of human diseases of accelerated aging(21). A common thread linking these disorders is that they all result from mutations in genes that are involved in genome maintenance. This strongly suggests that DNA damage can promote age-related degenerative changes.

ERCC1-XPF is a structure-specific endonuclease involved in the repair of several types of DNA lesions including interstrand crosslinks, double-strand breaks, and bulky, helix-distorting lesions(22, 23). ERCC1 and XPF are obligate binding partners and stabilize one another *in vivo*(24). Mutations in *XPF* that cause reduced expression of ERCC1-XPF cause a progeroid syndrome characterized by dramatically accelerated aging of most organ systems(24). *Ercc1*$^{-/-}$ and *Xpf*$^{-/-}$ mice have an identical phenotype to one another and mimic the human progeroid syndrome(25, 26). These mice die in the 4th week of life with aging-like degenerative changes, including osteoporosis, neurodegeneration, bone marrow hypoplasia, epidermal atrophy, sarcopenia, and liver and kidney dysfunction(24, 27). Liver dysfunction is life-limiting in *Ercc1*$^{-/-}$ mice(28). Mice with reduced but not ablated ERCC1-XPF expression live longer than *Ercc1*$^{-/-}$ mice (30 weeks vs. 4 weeks maxiumum lifespan)(29, 30) The *Ercc1*$^{-/\Delta}$ mice are healthy into adulthood (8 weeks) then begin to show numerous progressive symptoms associated with aging(30). The aim of this study was to systematically compare the liver of 4–5 month-old *Ercc1*$^{-/\Delta}$ mice to that of old WT mice (2+ yrs old) to determine if the progeroid mice offer an accurate model of natural aging that could be used to accelerate research on the biology of aging-related liver changes and therapeutic interventions to extend healthspan.

EXPERIMENTAL PROCEDURES

Animal Care and Experimentation

Experiments involving mice were approved by the University of Pittsburgh Institutional Animal Care and Use Committee and in accordance with the NIH guidelines for humane care of animals. *Ercc1*$^{-/\Delta}$ mice were bred and genotyped as previously described(23). All mice used in this study were in an f1 mixed genetic background (FVB/n:C57Bl/6).

Histological analyses

6–7 and 20–24 week old WT and *Ercc1*$^{-/\Delta}$ mice, along with aged (26–36 month) WT mice were sacrificed by CO_2 inhalation, and excised livers were fixed with 10% formalin and embedded in paraffin. Tissue sections (6μm) were cut and stained with hematoxylin and eosin (H&E) to detect changes in liver architecture and Masson's trichrome to detect fibrosis, using standard procedures. Alternatively liver specimens were cryopreserved by fixation in 10% formalin for 2–4 hours, followed by incubation in 30% sucrose at 4°C overnight. Tissues were embedded in OCT and flash frozen prior to sectioning on a Microm cryostat.

Liver Perfusion and Processing for Ultrastructural Analysis

For scanning and transmission electron microscopy, the liver of euthanized animals was cleared of blood by perfusion with phosphate-buffered saline (PBS) at 3mL/min through the inferior vena cava as previously described(31). Samples of liver were fixed with glutaraldehyde and processed also as described previously(32). TEM images were captured with the JEOL JEM 1011 microscope and SEM images were taken with the JEOL JSM 6330F microscope (JEOL Ltd, Peabody, MA). Porosity was determined using MetaMorph imaging software. Fenestrations were manually predetermined and porosity expressed as percent of measured total sinusoid area.

Immunofluorescence Analyses

Staining for acrolein was performed on deparaffinized liver sections from 20 wk-old WT, *Ercc1*$^{-/\Delta}$ mice and aged (24–36 mth-old) WT mice. Paraffin embedded tissue sections were subjected to heat induced-epitope retrieval by incubation in sodium citrate buffer (10mM, pH 6.0) for 10 min in a microwave, followed by 30 min cool-down. Sections were

permeabilized with PBS-Tween (0.05%) and incubated with rabbit polyclonal to acrolein (1:500, ab37110, Abcam, Cambridge, MA), CD31 (1:500, 550274, BD Pharmingen, San Diego, CA), F4/80 (1:500, 552958, BD Pharmingen, San Diego, CA), α-SMA (1:500, #6198, Sigma, St. Louis, MO), and Desmin (1:250, ab15200, Abcam, Cambridge, MA) overnight at 4°C. The secondary antibody, Alexa Fluor 594 goat anti-rabbit IgG (1:1000, A11012, Molecular Probes, Eugene, OR), was allowed to incubate for 60 min in the dark. Nuclei were stained with Vectashield with DAPI mounting medium (Vector Laboratories, Inc., Burlingame, CA). Ten random images per sample were acquired using an Olympus BX51 fluorescent microscope. Acrolein fluorescence intensity was quantified using the Axio Vision imaging software (Carl Zeiss, Gottingen, Germany). Average fluorescence intensity is shown ± S.E.M. All p-values reported were derived using a standard Student's *t* test with a two-tailed distribution. Differences were considered significant at the 95% confidence interval ($p < 0.05$).

Immunohistochemical analyses

Immunohistochemistry for Ki67 (rat anti-mouse Ki67 (TEC-3), Dako Cytomation, Carpinteria, CA) was performed on deparaffinized liver sections from 10 wk-old WT and *Ercc1*$^{-/\Delta}$ mice that had undergone partial hepatectomy surgery. Endogenous peroxidase activity was blocked with 3% hydrogen peroxide. Tissue sections were subjected to heat induced-epitope retrieval by incubation in sodium citrate buffer (10mM, pH 6.0) for 30 min in a decloaker, followed by 30 min cool-down. Blocking was done with 5% rabbit serum for 20 min. Primary antibody was applied for 1 hour. Secondary antibody was applied for 30 minutes, followed by the label antibody (ABC Elite, Vector Laboratories, Burlingame, CA) for 30 min. DAB chromagen (Dako Cytomation, Carpinteria, CA) was applied for 6 min, followed by 2 rinse steps in distilled water. Hematoxylin was used as a counterstain. Brightfield images were collected using an Olympus BX51 fluorescent microscope, and Ki67 positive cells were quantified from 5 random fields of view from each of 4 mice per group. Mean percentages were plotted ± S.E.M.; asterisk indicates $p<0.05$ as calculated with the Student's *t* test with a two-tailed distribution.

Detection of Lipids

Slides with frozen liver tissue were warmed to room temperature, fixed in 2% PFA for 10 min, rinsed with PBS, and incubated with LipidTox Red Neutral Lipid Stain (Invitrogen, Foster City, CA) for 30 min at room temperature. Tissues were rinsed in PBS and nuclei were counterstained with Hoechst dye for 1 min. Hoechst dye was rinsed off with 3 PBS washes and tissue was covered using gelvatol mounting medium. Image acquisition was done on an Olympus BX51 fluorescent microscope.

See Supplemental information for additional Experimental Procedures.

RESULTS

Histopathological changes in progeroid *Ercc1*$^{-/\Delta}$ mouse liver mimic normal aging

To investigate structural changes in the liver of progeroid *Ercc1*$^{-/\Delta}$ mice we compared liver tissue of 20–24 week-old *Ercc1*$^{-/\Delta}$ mice to wild-type (WT) littermates and to 26–34 month old WT mice. The relative liver/body weight of *Ercc1*$^{-/\Delta}$ mice was not significantly different from littermate controls at any age(30). The architecture of the *Ercc1*$^{-/\Delta}$ liver was irregular, with mild to moderate variation in lobular size (Figure 1A). Pathologic changes detected in both *Ercc1*$^{-/\Delta}$ mice and old WT mice include multifocal degeneration, necrosis and neutrophilic inflammation, a diffuse increase in sinusoidal lining cells, and karyomegaly, with intranuclear inclusions (Figure 1 and Supplemental Figure 1). None of these changes were detected in young adult (20–24 week-old) WT mice. The only

abnormalities detected in juvenile (7 wk-old) *Ercc1*$^{-/\Delta}$ mice were mild anisokaryosis and intranuclear inclusions. Liver from aged WT mice, like humans, displays mild portal fibrosis (Figure 1B) and increased neutral lipid accumulation (Figure 1C). Similar changes were detected in 20–24 wk-old *Ercc1*$^{-/\Delta}$ mice, but not age-matched WT mice or 7 wk-old *Ercc1*$^{-/\Delta}$ mice. This demonstrates that the *Ercc1*$^{-/\Delta}$ mice undergo progressive degenerative processes, rather than having developmental liver abnormalities.

Stellate cells are pericytes that reside between hepatocytes and endothelial cells lining the sinusoids in the extracellular space of Disse. Stellate cells store fat and when activated produce extracellular matrix proteins, contributing to fibrosis. With aging in humans, stellate cell number, but not activity is reported to increase(35). Similar results were found in 3 year-old WT mice and progeroid *Ercc1*$^{-/\Delta}$ mice, as measured by desmin and α-smooth muscle actin (SMA) staining, markers of stellate cells and their activation, respectively (Figure 1D). Kupffer cells, resident liver macrophages, are also reported to increase in number and phagocytic activity with aging in humans (36). However, we did not detect increased F4/80 immunostaining, a macrophage marker, in liver sections of old WT or progeroid mice (Supplemental Figure 2).

Pseudocapillarization and defenestration in progeroid *Ercc1*$^{-/\Delta}$ and old WT mouse liver

Age-associated endothelial changes in the liver are prominent and contribute to age-related decline in liver function(37). Expression of CD31, a marker of endothelium, was dramatically increased in 5 month-old *Ercc1*$^{-/\Delta}$ mice and 2.5 year-old WT mice compared to young adult WT mice (Figure 2A), indicative of pseudocapillarization. Pseudocapillarization encompasses many alterations including thickening of the sinusoidal endothelial cells (LSECs) and increased deposition of basement membrane proteins in the space of Disse(13, 38). Transmission electron microscopy of liver from old and progeroid mice revealed a thickening of the basement membrane (Figure 2B). This was confirmed by immunblot detection of the basement membrane protein laminin, which revealed a dramatically increased level of laminin in old WT and 20 week-old *Ercc1*$^{-/\Delta}$ mouse liver compared to young adult WT mice (Figure 2C).

With advanced age LSECs also lose their fenestrations, necessary for lipoprotein filtration, endocytosis, and immunological functions(37). Scanning electron microscopy of murine liver sections revealed a significant reduction in fenestration of the sinusoids in old (26–30 month-old) WT mice compared to young (20 week-old) WT animals (Figure 3A). Micrographs from 20 week-old *Ercc1*$^{-/\Delta}$ mice looked more similar to those from the old WT mice than to their WT littermates, with significantly reduced fenestrations, decreased porosity, and loss of sieve plates (Figure 3A–3B).

Age-related LSEC defenestration can lead to impaired hepatic clearance of atherogenic lipoproteins, contributing to hypertriglyceridemia, hypercholesteremia and vascular disease(39, 40). Therefore we measured serum cholesterol levels in the mice. Cholesterol levels were normal in young (7 wk-old) *Ercc1*$^{-/\Delta}$ mice (Figure 3C). By 21 weeks of age, when defenestration was apparent, serum cholesterol was significantly elevated in *Ercc1*$^{-/\Delta}$ mice compared to WT littermates. In contrast, serum triglycerides were significantly lower in 21 week-old compared to littermate controls (Figure 3D). Serum lipoproteins were not significantly altered in old WT mice compared to young WT mice.

Functional changes in progeroid *Ercc1*$^{-/\Delta}$ mouse liver mimic normal aging

Under normal conditions hepatocytes are quiescent cells, but can be stimulated to proliferate in response to parenchymal damage(41). In an experimental setting, proliferation is induced by partial hepatectomy (PHx), which leads to compensatory hyperplasia. Hepatocyte

proliferation in response to PHx is significantly decreased in aged rodents compared to young animals(8). Thirty-percent of the liver was surgically resected from 10 wk-old WT and *Ercc1*$^{-/\Delta}$ mice. *Ercc1*$^{-/\Delta}$ mice did not survive a standard PHx, which removes 70% of the liver. Thus the surgery was modified to only remove 1 lobe, or 30% of the liver. At 48 hours post-resection, the mice were euthanized and liver tissue collected for analysis. Previous experiments in which WT mice were euthanized every 12 hours post-partial hepatectomy, from 12–72 hours, indicated that 48 hours was the time point at which proliferation was the highest in 10 week-old WT mice (data not shown). Immunohistochemical staining for the proliferation-associated antigen Ki67 revealed a significant decrease in the number of proliferating cells in the liver from *Ercc1*$^{-/\Delta}$ mice compared to WT littermates (Figure 4A). Therefore regenerative capacity of the liver is prematurely reduced in *Ercc1*$^{-/\Delta}$ mice.

To further monitor liver function and integrity, liver function tests were performed on plasma of *Ercc1*$^{-/\Delta}$ and WT mice at multiple ages (Figure 4B). ALT was significantly elevated in old WT mice compared to young, as previously reported(42). ALT was also significantly elevated in *Ercc1*$^{-/\Delta}$ mice compared to age-matched WT mice, even at 7 wks of age. ALT levels more than doubled as the *Ercc1*$^{-/\Delta}$ mice aged. AST was also significantly elevated in old WT and 21 wk-old *Ercc1*$^{-/\Delta}$ mice compared to young adult WT mice. Serum albumin is known to decrease with age in humans and rodents(43, 44). Albumin was significantly reduced in the plasma of 21 wk-old, but not 7 wk-old *Ercc1*$^{-/\Delta}$ mice (Figure 4B). Thus, a very similar pattern of time-dependent changes in liver function tests, indicative of chronic, progressive tissue degeneration and loss of organ function, are observed in *Ercc1*$^{-/\Delta}$ and WT mice. However, the changes are dramatically accelerated in the *Ercc1*$^{-/\Delta}$ mice.

Increased cellular senescence in *Ercc1*$^{-/\Delta}$ and old WT liver

To further investigate the mechanism driving the loss of regenerative capacity in *Ercc1*$^{-/\Delta}$ and old WT mice, we asked if hepatocytes were undergoing cellular senescence. Liver sections were stained to detect senescence-associated β-galactosidase (SA-β gal) activity, a marker of cellular senescence (Figure 5A). SA-β Gal staining was increased in liver of 20 week-old *Ercc1*$^{-/\Delta}$ and old WT mice compared to 20 week-old WT mice. p16^{INK4a} is another established marker of senescent cells(45). p16^{INK4a} expression was increased 1.4- and 2.0-fold in 20 wk-old *Ercc1*$^{-/\Delta}$ and 2 yr-old WT mice, respectively, compared to young WT mice (Figure 5B). Increased cell size, nuclear size, and the nuclear:cytoplasmic ratio are also associated with cell senescence and old age(46–48). The nuclear size of hepatocytes was heterogeneous in *Ercc1*$^{-/\Delta}$ and old WT mice compared to 7 and 23 wk-old WT mice (Figure 5C). Hepatocyte nuclei of *Ercc1*$^{-/\Delta}$ mice were significantly larger than that of WT littermates at 7 wks of age, and increased by 21 wks of age (Figure 5C). Nuclear size was also significantly increased in old WT mice compared to young WT mice. Electron micrographs revealed a highly irregular surface area of the hepatocyte nuclei from *Ercc1*$^{-/\Delta}$ and old, but not young, WT mice (Figure 5D).

Increased oxidative damage in *Ercc1*$^{-/\Delta}$ liver is also found with natural aging

Oxidative stress has been implicated in driving age-dependent cellular senescence(49). To determine if oxidative stress is elevated in *Ercc1*$^{-/\Delta}$ mice and with old age, we measured lipid peroxidation in liver. The level of lipid hydroperoxides, measured by ELISA, was elevated in the liver of 20 wk-old *Ercc1*$^{-/\Delta}$ mice compared to WT littermates (Figure 6A). A similar elevation was seen in old WT mouse liver compared to young WT. This increase in lipid peroxidation was confirmed by immunodetection of acrolein, a stable product of lipid peroxidation. *Ercc1*$^{-/\Delta}$ and old WT mice had significantly increased acrolein compared to adult WT mice (Figure 6B).

One of the most common markers of aged liver is the cytoplasmic accumulation of lipofuscin, which is highly oxidized lipid material(11). Lipofuscin granules, which fluoresce at 488nm, were 30-fold elevated in liver of 20 week-old *Ercc1*$^{-/\Delta}$ mice compared to WT littermates (Figure 6C). A similar increase in lipofuscin was observed in old WT mouse liver compared to young WT mice.

Transcriptional changes in *Ercc1*$^{-/\Delta}$ mouse liver parallels natural aging

Gene expression changes were measured by microarray in liver of *Ercc1*$^{-/\Delta}$ mice and WT littermates at 5 and 16 weeks of age. Genes that were significantly up or downregulated compared to WT littermates are shown (Figure 7A). There is a progressive downregulation of genes associated with the IGF-1/GH axis and oxidative phosphorylation in *Ercc1*$^{-/\Delta}$ mice as they age compared to WT littermates. Additionally, genes involved in DNA damage, oxidative stress response, cell cycle arrest, and apoptosis were significantly upregulated in 16 week-old *Ercc1*$^{-/\Delta}$ mice compared to WT littermates. qPCR was used to confirm the microarray results (Figure 7B).

The transcriptional changes observed in 16 week-old *Ercc1*$^{-/\Delta}$ mouse liver are comparable to old WT (130 week) mice (Figure 7C). Spearman's r correlation indicates that as *Ercc1*$^{-/\Delta}$ progeroid mice age from 5 weeks to 16 weeks, their gene expression profiles have increasing similarity to old WT mice.

DISCUSSION

The human liver undergoes numerous characteristic structural and functional changes with increasing age(13). Structural changes include loss of organ volume, nuclear polyploidy, anisokaryosis, and pseuodcapillarization(13, 42, 50). These changes lead to impaired liver function and loss of regenerative capacity. Not surprisingly, transplanted livers from late-age donors have decreased graft acceptance and function(51, 52). However, the underlying cause for these changes remains unknown.

Non-human primates have been used to study liver aging, but the commonly used species *Macaca mulatta* and *Macaca nemestrina* can live more than 20 years(53, 54). Mice are shorter-lived and importantly age-related changes characteristic of aged human liver are recapitulated in mice, including pseudocapillarization, increased polyploidy, decreased hepatocyte number, and increased nuclear size(18–20, 55). Thus, mice represent an accurate model system for studying age-associated liver changes in humans. However, the 3 year lifespan of mice still represents a substantial barrier to rapid testing of hypotheses about the causes and treatments of liver aging.

Herein we establish that the structural, functional and regulatory changes that occur in the liver of WT mice in their third year of life are recapitulated in the *Ercc1*$^{-/\Delta}$ progeroid mouse strain within their 7-month lifespan. There is a highly significant correlation between the genome-wide expression profile of 4 month-old *Ercc1*$^{-/\Delta}$ mice and 32 month-old WT mice (Figure 7). Both have elevated LFTs and reduced regenerative capacity, as well as focal necrosis, inflammation, anisokaryosis, and steatosis (Figures 1 and 4). Markers of cellular senescence (SA-βgal and p16) are elevated in livers of progeroid and old mice (Figure 5). This is supported by the strong upregulation of genes associated with cell cycle arrest (Figure 7) and the observation that livers of *Ercc1*$^{-/\Delta}$ mice, like that of old WT mice(56–58) have reduced regenerative capacity following partial hepatectomy (Figure 4). Collectively, these data support the conclusion that age-related decrease of liver function is due to dysfunction of hepatocytes rather than their attrition. Interestingly, there is accumulation of oxidation products (lipofuscin and lipid peroxidation) in the livers of progeroid and old mice (Figure 6), suggesting that oxidative damage may drive hepatocyte dysfunction.

Defenestration and pseudocapillarization, which were significantly elevated in livers of *Ercc1*$^{-/\Delta}$ and old WT mice (Figures 2 and 3), contribute to reduced regenerative capacity(58). Defenestration is also implicated in dyslipidemia due to impaired clearance of lipoproteins from the blood to hepatocytes(39). Serum cholesterol was significantly elevated in progeroid *Ercc1*$^{-/\Delta}$ mice compared to littermate controls (Figure 3). In contrast, serum triglycerides were significantly lower in mutant animals compared to WT mice. Despite the fact that the extent of defenestration was similar in progeroid and old WT mice, serum lipid levels were within normal range in the naturally aged mice. Hence the dyslipidemia in the *Ercc1*$^{-/\Delta}$ mice may reflect metabolic changes in the mice rather than a loss of liver transport mechanisms. Indeed, metabolic profiling of the *Ercc1*$^{-/\Delta}$ mice revealed increased serum HDL but decreased LDL and VLDL and increased urinary ketone bodies(59). These changes mimic caloric restriction (60) and occur as a consequence genetic reprogramming rather than diminished nutrient intake in the *Ercc1*$^{-/\Delta}$ mice (Figure 7 and(59, 61)). The growth hormone/insulin-like growth factor-1 axis is also attenuated in *Ercc1*$^{-/\Delta}$ mice and old WT mice (Figure 7 and(24, 61)). This drives the metabolic shift and also contributes to impaired liver regeneration(62).

Ercc1$^{-/\Delta}$ mice age rapidly as a consequence of an engineered mutation in the gene that encodes one subunit of the DNA repair endonuclease ERCC1-XPF (63), which is required for multiple DNA repair pathways (22, 23). XFE progeroid syndrome, which the ERCC1-deficient mice model, is characterized by accelerated aging of the hematopoietic, hepatobiliary, endocrine, musculoskeletal and neurological systems(24, 27). Werner syndrome, caused by mutations in *WRN*, which encodes a DNA repair helicase and exonuclease, is characterized by early onset cancer, cardiovascular disease and osteoporosis(64). Both *Ercc1*$^{-/\Delta}$ and *Wrn*$^{\Delta hel/\Delta hel}$ mice display early onset of dyslipidemia, steatosis, pseudocapillarization and defenestration in the liver(65). This demonstrates that DNA repair is critical for protecting against loss of liver homeostasis and function. Importantly, levels of 8-oxo-deoxyguanine, an endogenous oxidative DNA lesion, are greater in old WT mice than young(66–68), consistent with the hypothesis that unrepaired DNA damage may contribute to liver aging even in repair-proficient organisms.

The mice in this study were not exposed to environmental genotoxins. Thus the degenerative changes observed are attributed to the accumulation of oxidative damage arising as a consequence of normal metabolism. The fact that the onset of degenerative changes are accelerated in DNA repair-deficient *Ercc1*$^{-/\Delta}$ mice compared to WT reveals that specifically endogenous DNA damage can drive liver degeneration, likely through driving hepatocyte senescence(69). In humans, environmental exposures as well as endogenously produced genotoxic by-products undoubtedly contribute to the accumulating burden of DNA damage and thereby age-related liver dysfunction.

It is important to note that many of the age-related endpoints measured were more severely affected in *Ercc1*$^{-/\Delta}$ mice than in WT mice near the end of their respective lifespans. This includes LFTs, fibrosis, steatosis, pseudocapillarization, and anisokaryosis. A unifying explanation for why the liver of 4–5 month-old Ercc1$^{-/\Delta}$ mice looks worse than 2–3 year-old WT mice is that the *Ercc1*$^{-/\Delta}$ mice undergo activation of stress response pathways, similar to that induced by caloric restriction, which are protective, as the result of accumulated, unrepaired DNA damage. (Figure 7 and (24, 61)). Thus the *Ercc1*$^{-/\Delta}$ mice survive longer than expected given their burden of damage and therefore have extreme aging, comparable to that of supercentenarians(30). Nevertheless, *Ercc1*$^{-/\Delta}$ mice develop the majority of structural and funtional characteristics of old human(13) and mouse liver within a matter of five months, rather than years. The vast majority of these changes occur in adulthood (after 7 weeks of age), making the changes distinct from developmental abnormalities and degenerative in nature. *Ercc1*$^{-/\Delta}$ mice therefore represent an accurate

model system for rapidly testing hypotheses about the mechanism underlying age-related liver degeneration and pharmacological interventions aimed at delaying or ameliorating age-associated liver disease.

Supplementary Material

Refer to Web version on PubMed Central for supplementary material.

List of Abbreviations

CDC	Center for Disease Control
WHO	World Health Organization
ERCC	excision repair cross complementation group 1
LSEC	liver sinusoidal endothelial cells
WT	Wild-type
H&E	Haematoxylin & Eosin
α-SMA	alpha smooth muscle actin
SEM	Scanning electron microscopy
TEM	Transmission electron microscopy
AST	Aspartate transaminase
ALT	Alanine transaminase
SA β-gal	senescence-associated β-galactosidase

Acknowledgments

Financial Support: We thank Chelsea Feldman, Cheryl Clauson and members of the Niedernhofer lab for experimental support and critical reading of the manuscript. This work was supported by the National Institutes of Health grants ES016114 and -032 to L.J.N. and CA076541 to D.B.S., the Ellison Medical Foundation (AG-NS-0303-05; L.J.N.), and Pilot Projects from the University of Pittsburgh Claude B. Pepper Center (P30AG024827; PI: Studenski) and a Pilot the Pittsburgh Center for Kidney Research (P30DK079307; PI Kleyman). This project used the UPCI Cell and Tissue Imaging and Animal Facilities and was supported in part by award P30CA047904.

REFERENCES

1. Kirkwood TB. Understanding the odd science of aging. Cell. 2005; 120:437–447. [PubMed: 15734677]
2. Xu, J.; Kochanek, KD.; Murphy, SL.; Tejada-Vera, B. Services USDoHaH, editor. Hyattsville, MD: 2010. Deaths: Final Data for 2007.
3. del Olmo JA, Serra MA, Rodriguez F, Escudero A, Gilabert S, Rodrigo JM. Incidence and risk factors for hepatocellular carcinoma in 967 patients with cirrhosis. J Cancer Res Clin Oncol. 1998; 124:560–564. [PubMed: 9829860]
4. Frith J, Jones D, Newton JL. Chronic liver disease in an ageing population. Age Ageing. 2009; 38:11–18. [PubMed: 19029099]
5. Wynne HA, Cope LH, Mutch E, Rawlins MD, Woodhouse KW, James OF. The effect of age upon liver volume and apparent liver blood flow in healthy man. Hepatology. 1989; 9:297–301. [PubMed: 2643548]
6. Popper H. Aging and the liver. Prog Liver Dis. 1986; 8:659–683. [PubMed: 3520674]
7. Michalopoulos GK. Liver regeneration. J Cell Physiol. 2007; 213:286–300. [PubMed: 17559071]

8. Bucher NL, Swaffield MN, Ditroia JF. The Influence of Age Upon the Incorporation of Thymidine-2-C14 into the DNA of Regenerating Rat Liver. Cancer Res. 1964; 24:509–512. [PubMed: 14147827]
9. Chipchase MD, O'Neill M, Melton DW. Characterization of premature liver polyploidy in DNA repair (Ercc1)-deficient mice. Hepatology. 2003; 38:958–966. [PubMed: 14512883]
10. Andrew W. An electron microscope study of age changes in the liver of the mouse. Am J Anat. 1962; 110:1–18. [PubMed: 13861468]
11. Schmucker DL, Sachs H. Quantifying dense bodies and lipofuscin during aging: a morphologist's perspective. Arch Gerontol Geriatr. 2002; 34:249–261. [PubMed: 14764327]
12. Jung T, Bader N, Grune T. Lipofuscin: formation, distribution, and metabolic consequences. Ann N Y Acad Sci. 2007; 1119:97–111. [PubMed: 18056959]
13. McLean AJ, Cogger VC, Chong GC, Warren A, Markus AM, Dahlstrom JE, Le Couteur DG. Age-related pseudocapillarization of the human liver. J Pathol. 2003; 200:112–117. [PubMed: 12692849]
14. Kagansky N, Levy S, Keter D, Rimon E, Taiba Z, Fridman Z, Berger D, et al. Non-alcoholic fatty liver disease--a common and benign finding in octogenarian patients. Liver Int. 2004; 24:588–594. [PubMed: 15566509]
15. Adams LA, Angulo P. Recent concepts in non-alcoholic fatty liver disease. Diabet Med. 2005; 22:1129–1133. [PubMed: 16108837]
16. Warren A, Bertolino P, Cogger VC, McLean AJ, Fraser R, Le Couteur DG. Hepatic pseudocapillarization in aged mice. Exp Gerontol. 2005; 40:807–812. [PubMed: 16125353]
17. Hoare M, Das T, Alexander G. Ageing, telomeres, senescence, and liver injury. J Hepatol. 2010; 53:950–961. [PubMed: 20739078]
18. Ito Y, Sorensen KK, Bethea NW, Svistounov D, McCuskey MK, Smedsrod BH, McCuskey RS. Age-related changes in the hepatic microcirculation in mice. Exp Gerontol. 2007; 42:789–797. [PubMed: 17582718]
19. Ohtsubo K, Nomaguchi TA. A flow cytofluorometric study on age-dependent ploidy class changes in mouse hepatocyte nuclei. Mech Ageing Dev. 1986; 36:125–131. [PubMed: 3784626]
20. Pieri C, Giuli C, Del Moro M, Piantanelli L. Electron-microscopic morphometric analysis of mouse liver. II. Effect of ageing and thymus transplantation in old animals. Mech Ageing Dev. 1980; 13:275–283. [PubMed: 7421302]
21. Hasty P, Campisi J, Hoeijmakers J, van Steeg H, Vijg J. Aging and genome maintenance: lessons from the mouse? Science. 2003; 299:1355–1359. [PubMed: 12610296]
22. Niedernhofer LJ, Odijk H, Budzowska M, van Drunen E, Maas A, Theil AF, de Wit J, et al. The structure-specific endonuclease Ercc1-Xpf is required to resolve DNA interstrand cross-link-induced double-strand breaks. Mol Cell Biol. 2004; 24:5776–5787. [PubMed: 15199134]
23. Ahmad A, Robinson AR, Duensing A, van Drunen E, Beverloo HB, Weisberg DB, Hasty P, et al. ERCC1-XPF endonuclease facilitates DNA double-strand break repair. Mol Cell Biol. 2008; 28:5082–5092. [PubMed: 18541667]
24. Niedernhofer LJ, Garinis GA, Raams A, Lalai AS, Robinson AR, Appeldoorn E, Odijk H, et al. A new progeroid syndrome reveals that genotoxic stress suppresses the somatotroph axis. Nature. 2006; 444:1038–1043. [PubMed: 17183314]
25. McWhir J, Selfridge J, Harrison DJ, Squires S, Melton DW. Mice with DNA repair gene (ERCC-1) deficiency have elevated levels of p53, liver nuclear abnormalities and die before weaning. Nat Genet. 1993; 5:217–224. [PubMed: 8275084]
26. Tian M, Shinkura R, Shinkura N, Alt FW. Growth retardation, early death, and DNA repair defects in mice deficient for the nucleotide excision repair enzyme XPF. Mol Cell Biol. 2004; 24:1200–1205. [PubMed: 14729965]
27. Prasher JM, Lalai AS, Heijmans-Antonissen C, Ploemacher RE, Hoeijmakers JH, Touw IP, Niedernhofer LJ. Reduced hematopoietic reserves in DNA interstrand crosslink repair-deficient Ercc1−/− mice. EMBO J. 2005; 24:861–871. [PubMed: 15692571]
28. Selfridge J, Hsia KT, Redhead NJ, Melton DW. Correction of liver dysfunction in DNA repair-deficient mice with an ERCC1 transgene. Nucleic Acids Res. 2001; 29:4541–4550. [PubMed: 11713303]

29. de Waard MC, van der Pluijm I, Zuiderveen Borgesius N, Comley LH, Haasdijk ED, Rijksen Y, Ridwan Y, et al. Age-related motor neuron degeneration in DNA repair-deficient Ercc1 mice. Acta Neuropathol. 2010; 120:461–475. [PubMed: 20602234]
30. Dolle MET, Kuiper RV, Roodbergen M, Robinson J, de Vlugt S, Wijnhoven SWP, Beems RB, de la Fonteyne L, de With P, van der Pluijm I, Niedernhofer LJ, Hasty P, Vijg J, Hoeijmakers JHJ, Harry van Steeg. Broad segmental progeroid changes in short-lived Ercc1−/Δ7 mice. Pathobiology of Aging and Age-related diseases. 2011; 1:7219.
31. Seglen PO. Preparation of isolated rat liver cells. Methods Cell Biol. 1976; 13:29–83. [PubMed: 177845]
32. Wack KE, Ross MA, Zegarra V, Sysko LR, Watkins SC, Stolz DB. Sinusoidal ultrastructure evaluated during the revascularization of regenerating rat liver. Hepatology. 2001; 33:363–378. [PubMed: 11172338]
33. Mitchell C, Willenbring H. A reproducible and well-tolerated method for 2/3 partial hepatectomy in mice. Nat Protoc. 2008; 3:1167–1170. [PubMed: 18600221]
34. Dimri GP, Lee X, Basile G, Acosta M, Scott G, Roskelley C, Medrano EE, et al. A biomarker that identifies senescent human cells in culture and in aging skin in vivo. Proc Natl Acad Sci U S A. 1995; 92:9363–9367. [PubMed: 7568133]
35. Warren A, Cogger VC, Fraser R, Deleve LD, McCuskey RS, Le Couteur DG. The effects of old age on hepatic stellate cells. Curr Gerontol Geriatr Res. 2011; 2011:439835. [PubMed: 21687587]
36. Hilmer SN, Cogger VC, Le Couteur DG. Basal activity of Kupffer cells increases with old age. J Gerontol A Biol Sci Med Sci. 2007; 62:973–978. [PubMed: 17895435]
37. Le Couteur DG, Warren A, Cogger VC, Smedsrod B, Sorensen KK, De Cabo R, Fraser R, et al. Old age and the hepatic sinusoid. Anat Rec (Hoboken). 2008; 291:672–683. [PubMed: 18484614]
38. Le Couteur DG, Cogger VC, Markus AM, Harvey PJ, Yin ZL, Ansselin AD, McLean AJ. Pseudocapillarization and associated energy limitation in the aged rat liver. Hepatology. 2001; 33:537–543. [PubMed: 11230732]
39. Le Couteur DG, Cogger VC, McCuskey RS, R DEC, Smedsrod B, Sorensen KK, Warren A, et al. Age-related changes in the liver sinusoidal endothelium: a mechanism for dyslipidemia. Ann N Y Acad Sci. 2007; 1114:79–87. [PubMed: 17804522]
40. Hilmer SN, Cogger VC, Fraser R, McLean AJ, Sullivan D, Le Couteur DG. Age-related changes in the hepatic sinusoidal endothelium impede lipoprotein transfer in the rat. Hepatology. 2005; 42:1349–1354. [PubMed: 16317689]
41. Fausto N, Campbell JS, Riehle KJ. Liver regeneration. Hepatology. 2006; 43:S45–S53. [PubMed: 16447274]
42. Schmucker DL. Age-related changes in liver structure and function: Implications for disease ? Exp Gerontol. 2005; 40:650–659. [PubMed: 16102930]
43. Kitani K. Liver and aging. Gastroenterol Jpn. 1992; 27:276–285. [PubMed: 1577235]
44. Vranckx R, Savu L, Lambert N, de Conchard GV, Grosse R, Mourey MS, Corman B. Plasma proteins as biomarkers of the aging process. Am J Physiol. 1995; 268:R536–R548. [PubMed: 7532377]
45. Alcorta DA, Xiong Y, Phelps D, Hannon G, Beach D, Barrett JC. Involvement of the cyclin-dependent kinase inhibitor p16 (INK4a) in replicative senescence of normal human fibroblasts. Proc Natl Acad Sci U S A. 1996; 93:13742–13747. [PubMed: 8943005]
46. Rodier F, Campisi J. Four faces of cellular senescence. J Cell Biol. 2011; 192:547–556. [PubMed: 21321098]
47. Sherwood SW, Rush D, Ellsworth JL, Schimke RT. Defining cellular senescence in IMR-90 cells: a flow cytometric analysis. Proc Natl Acad Sci U S A. 1988; 85:9086–9090. [PubMed: 3194411]
48. Moraes AS, Guaraldo AM, Mello ML. Chromatin supraorganization and extensibility in mouse hepatocytes with development and aging. Cytometry A. 2007; 71:28–37. [PubMed: 17211882]
49. Ben-Porath I, Weinberg RA. The signals and pathways activating cellular senescence. Int J Biochem Cell Biol. 2005; 37:961–976. [PubMed: 15743671]
50. Watanabe T, Shimada H, Tanaka Y. Human hepatocytes and aging: a cytophotometrical analysis in 35 sudden-death cases. Virchows Arch B Cell Pathol. 1978; 27:307–316. [PubMed: 98902]

51. Busquets J, Xiol X, Figueras J, Jaurrieta E, Torras J, Ramos E, Rafecas A, et al. The impact of donor age on liver transplantation: influence of donor age on early liver function and on subsequent patient and graft survival. Transplantation. 2001; 71:1765–1771. [PubMed: 11455256]
52. Hoofnagle JH, Lombardero M, Zetterman RK, Lake J, Porayko M, Everhart J, Belle SH, et al. Donor age and outcome of liver transplantation. Hepatology. 1996; 24:89–96. [PubMed: 8707288]
53. Maloney AG, Schmucker DL, Vessey DS, Wang RK. The effects of aging on the hepatic microsomal mixed-function oxidase system of male and female monkeys. Hepatology. 1986; 6:282–287. [PubMed: 3082734]
54. Sutter MA, Wood WG, Williamson LS, Strong R, Pickham K, Richardson A. Comparison of the hepatic mixed function oxidase system of young, adult, and old non-human primates (Macaca nemestrina). Biochem Pharmacol. 1985; 34:2983–2987. [PubMed: 4026880]
55. Stuart GR, Oda Y, de Boer JG, Glickman BW. Mutation frequency and specificity with age in liver, bladder and brain of lacI transgenic mice. Genetics. 2000; 154:1291–1300. [PubMed: 10757770]
56. Wang X, Quail E, Hung NJ, Tan Y, Ye H, Costa RH. Increased levels of forkhead box M1B transcription factor in transgenic mouse hepatocytes prevent age-related proliferation defects in regenerating liver. Proc Natl Acad Sci U S A. 2001; 98:11468–11473. [PubMed: 11572993]
57. Wang X, Krupczak-Hollis K, Tan Y, Dennewitz MB, Adami GR, Costa RH. Increased hepatic Forkhead Box M1B (FoxM1B) levels in old-aged mice stimulated liver regeneration through diminished p27Kip1 protein levels and increased Cdc25B expression. J Biol Chem. 2002; 277:44310–44316. [PubMed: 12221098]
58. Furrer K, Rickenbacher A, Tian Y, Jochum W, Bittermann AG, Kach A, Humar B, et al. Serotonin reverts age-related capillarization and failure of regeneration in the liver through a VEGF-dependent pathway. Proc Natl Acad Sci U S A. 2011; 108:2945–2950. [PubMed: 21282654]
59. Nevedomskaya E, Meissner A, Goraler S, de Waard M, Ridwan Y, Zondag G, van der Pluijm I, et al. Metabolic profiling of accelerated aging ERCC1 d/− mice. J Proteome Res. 2010; 9:3680–3687. [PubMed: 20507129]
60. Cruzen C, Colman RJ. Effects of caloric restriction on cardiovascular aging in non-human primates and humans. Clin Geriatr Med. 2009; 25:733–743. ix–x. [PubMed: 19944270]
61. Schumacher B, van der Pluijm I, Moorhouse MJ, Kosteas T, Robinson AR, Suh Y, Breit TM, et al. Delayed and accelerated aging share common longevity assurance mechanisms. PLoS Genet. 2008; 4:e1000161. [PubMed: 18704162]
62. Krupczak-Hollis K, Wang X, Dennewitz MB, Costa RH. Growth hormone stimulates proliferation of old-aged regenerating liver through forkhead box m1b. Hepatology. 2003; 38:1552–1562. [PubMed: 14647066]
63. Weeda G, Donker I, de Wit J, Morreau H, Janssens R, Vissers CJ, Nigg A, et al. Disruption of mouse ERCC1 results in a novel repair syndrome with growth failure, nuclear abnormalities and senescence. Curr Biol. 1997; 7:427–439. [PubMed: 9197240]
64. Muftuoglu M, Oshima J, von Kobbe C, Cheng WH, Leistritz DF, Bohr VA. The clinical characteristics of Werner syndrome: molecular and biochemical diagnosis. Hum Genet. 2008; 124:369–377. [PubMed: 18810497]
65. Labbe A, Garand C, Cogger VC, Paquet ER, Desbiens M, Le Couteur DG, Lebel M. Resveratrol improves insulin resistance hyperglycemia and hepatosteatosis but not hypertriglyceridemia, inflammation, and life span in a mouse model for Werner syndrome. Gerontol A Biol Sci Med Sci. 2010; 66:264–278.
66. Mikkelsen L, Bialkowski K, Risom L, Lohr M, Loft S, Moller P. Aging and defense against generation of 8-oxo-7,8-dihydro-2'-deoxyguanosine in DNA. Free Radic Biol Med. 2009; 47:608–615. [PubMed: 19500668]
67. Zahn RK, Zahn-Daimler G, Ax S, Reifferscheid G, Waldmann P, Fujisawa H, Hosokawa M. DNA damage susceptibility and repair in correlation to calendric age and longevity. Mech Ageing Dev. 2000; 119:101–112. [PubMed: 11080531]
68. Lopez-Diazguerrero NE, Luna-Lopez A, Gutierrez-Ruiz MC, Zentella A, Konigsberg M. Susceptibility of DNA to oxidative stressors in young and aging mice. Life Sci. 2005; 77:2840–2854. [PubMed: 15979101]

69. Rodier F, Coppe JP, Patil CK, Hoeijmakers WA, Munoz DP, Raza SR, Freund A, et al. Persistent DNA damage signalling triggers senescence-associated inflammatory cytokine secretion. Nat Cell Biol. 2009; 11:973–979. [PubMed: 19597488]

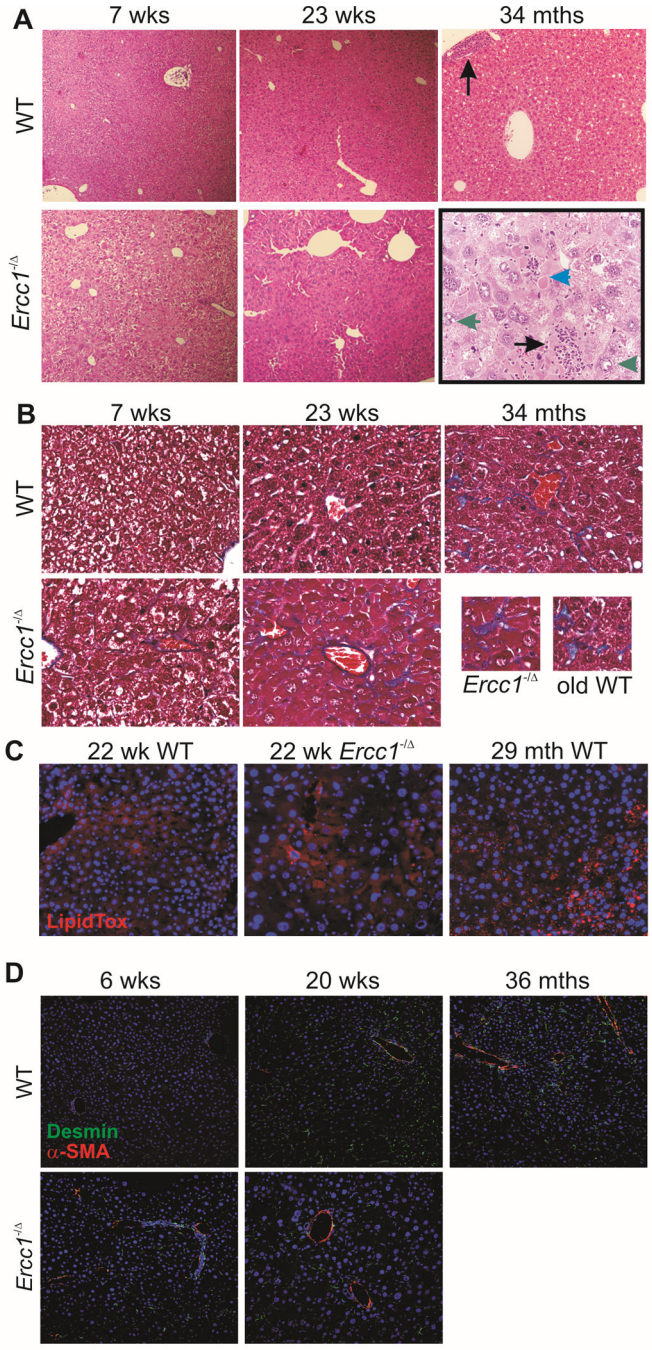

Figure 1. Premature onset of age-related pathology in *Ercc1*$^{-/\Delta}$ mouse liver

(A) Hematoxylin and eosin (H&E) stained liver sections from 7 wk, 23 wk, and 34 mth-old WT mice, and *Ercc1*$^{-/\Delta}$ littermates (10X). The bottom right panel is a high magnification (40X) image of *Ercc1*$^{-/\Delta}$ liver (23 wk) illustrating inflammatory infiltrate (black arrows), abnormal nuclei with inclusion (green arrows) and dead hepatocytes (blue arrows).

(B) Masson's trichrome stained liver sections. Insets (40X) in the bottom right panel show perisinusoidal fibrosis in *Ercc1*$^{-/\Delta}$ and old WT liver samples.

(C) LipidTOX™ stain of liver sections to detect neutral lipids (20X).

(D) Immunofluorescence detection of desmin and α-SMA, markers of hepatic stellate cells and their activation, respectively, in frozen liver sections (20X).

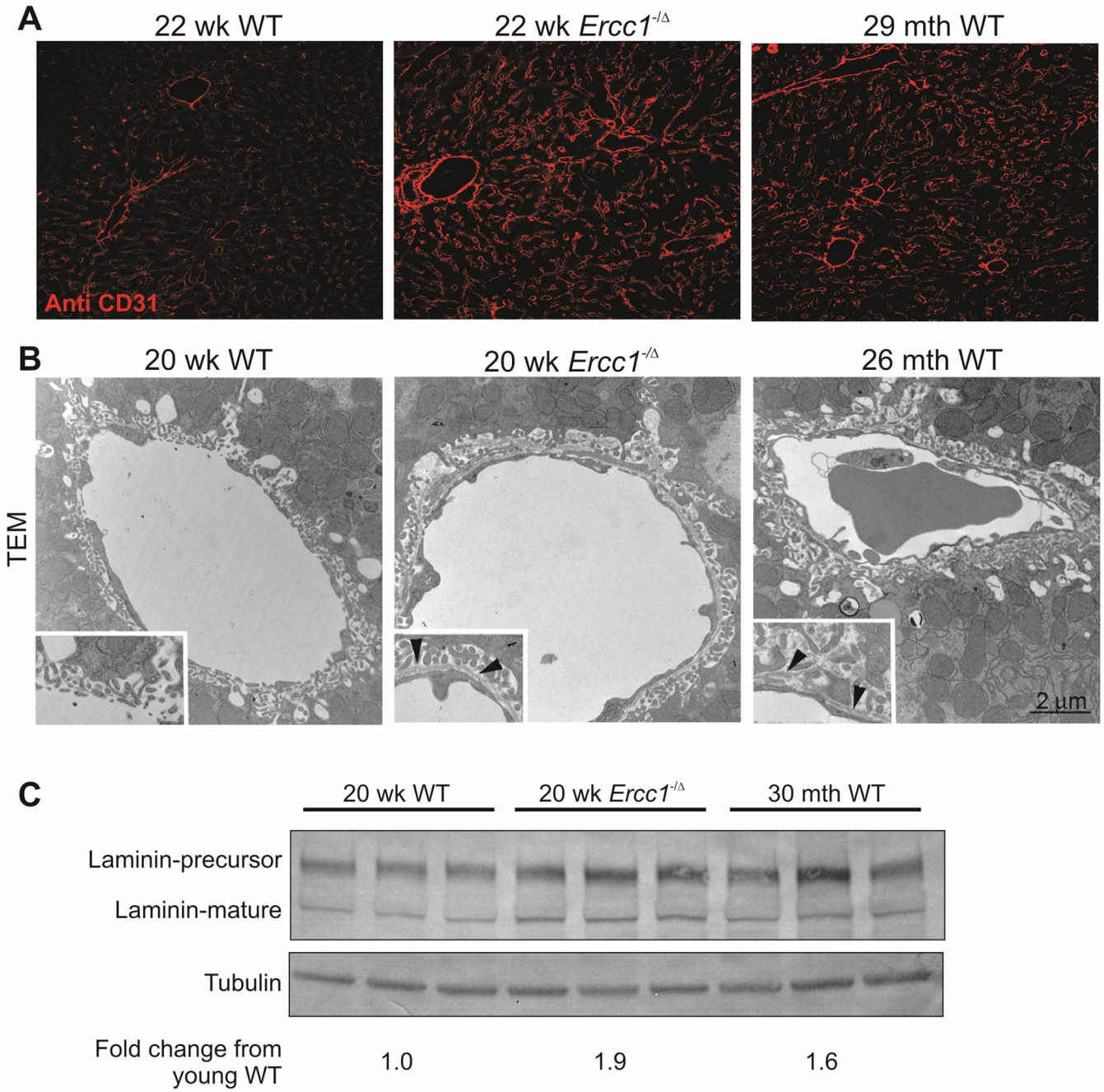

Figure 2. Age-related thickening of the sinusoidal endothelium in *Ercc1*$^{-/\Delta}$ mouse liver

(A) Immunofluorescence detection of CD31, a surface marker of endothelial cells in frozen liver sections (20X).

(B) Transmission electron micrographs (TEM; 12,000X) of liver illustrating thickening of the basement membrane in sinusoids of mutant and old WT mice compared to young WT. Insets show enlargement of a portion of the original image and arrows indicate deposition of basement membrane and pseudocapillarization of the sinusoidal endothelium.

(C) Immunoblot to detect the extracellular matrix protein laminin in liver lysates from 20 wk-old *Ercc1*$^{-/\Delta}$ mice, control littermates and old WT (2–3 year) mice (n=3 per group).

Densitometry was used for quantification and averages are listed as a ratio compared to 20 week-old WT mice.

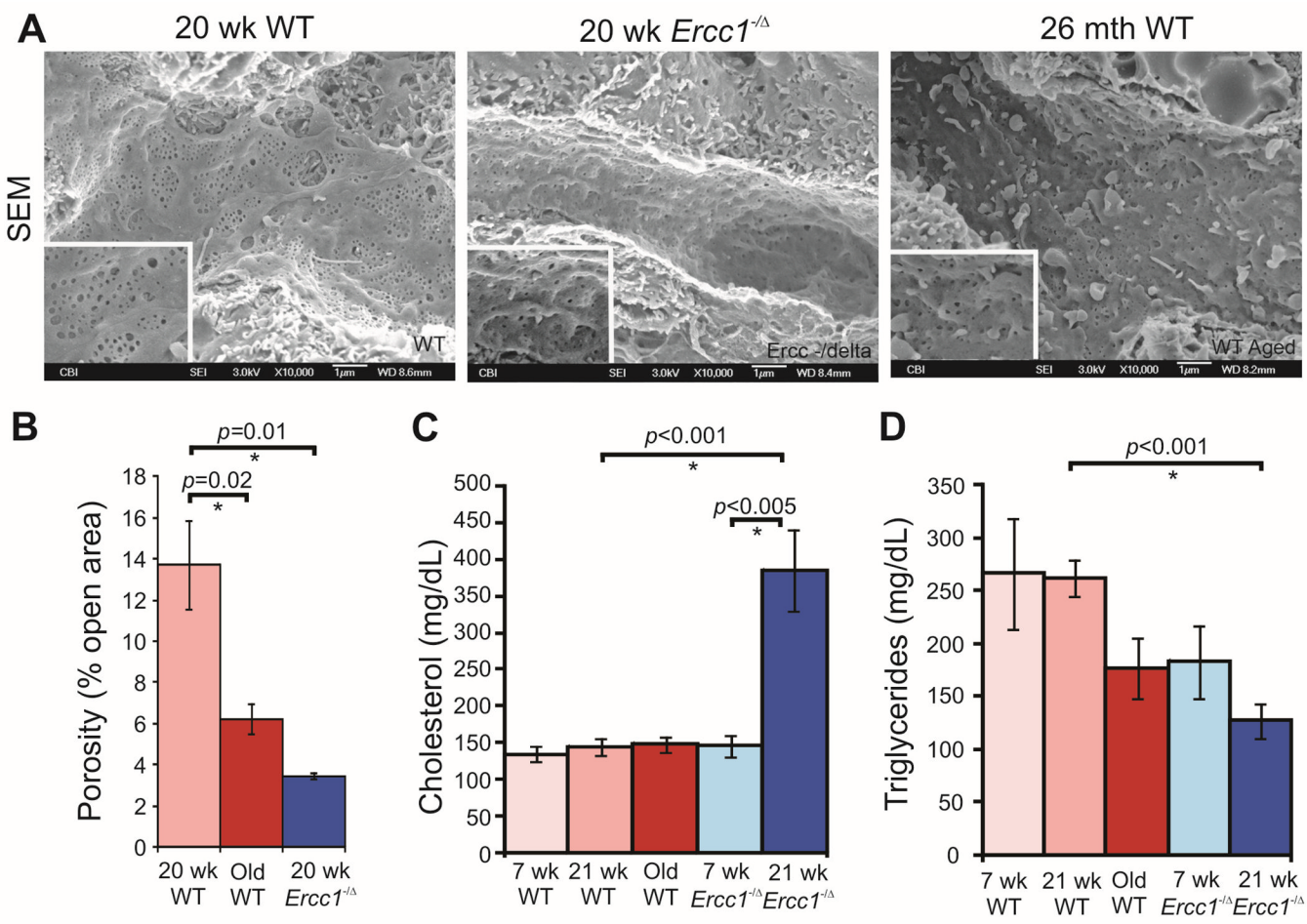

Figure 3. Premature defenestration in *Ercc1*$^{-/\Delta}$ mouse liver

(A) Scanning electron micrograph (10,000X) of liver, illustrating defenestration in sinusoids of mutant and old WT mice. Insets show enlargement of a portion of the original image.

(B) Quantification of porosity shown in A. 3 SEM images per mouse (n=3 mice per group) were quantified, and the % open area of the sinusoid is represented ± S.E.M. Asterisks indicate significant differences.

(C) Serum cholesterol and (D) triglyceride levels in WT and *Ercc1*$^{-/\Delta}$ mice of various ages. The average ± S.E.M. are plotted (n=6 for 7 wk-old mice, n=9 for 21 wk-old and old WT mice). Asterisks indicate significant differences as calculated by a paired Student's t test.

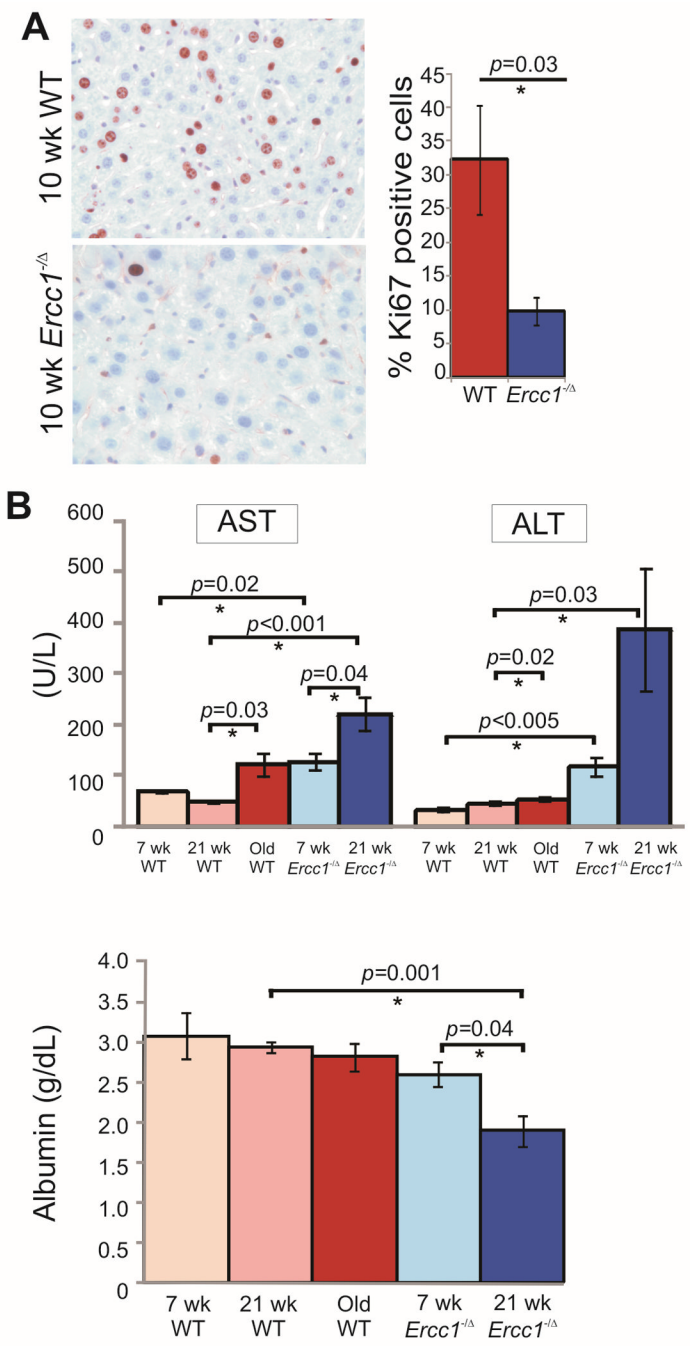

Figure 4. Premature loss of liver function in *Ercc1*$^{-/\Delta}$ mice

(A) Representative liver sections from 10 week-old WT and *Ercc1*$^{-/\Delta}$ mice immunostained for the proliferation marker Ki67 48 hr post-partial hepatectomy. The fraction of proliferating hepatocytes is graphed (5 random fields of view analyzed from n=4 mice per genotype; asterisk indicates p<0.05, Student's two tailed t-test).

(B) Serum chemistries reflecting liver function. Plotted are the average ± S.E.M. for 6 mice per age and genotype. WT animals are graphed in reds; *Ercc1*$^{-/\Delta}$ mice in blues. Darker colors indicate increasing age. AST is aspartate transminase; ALT is alanine transaminase. Asterisks indicate significant differences.

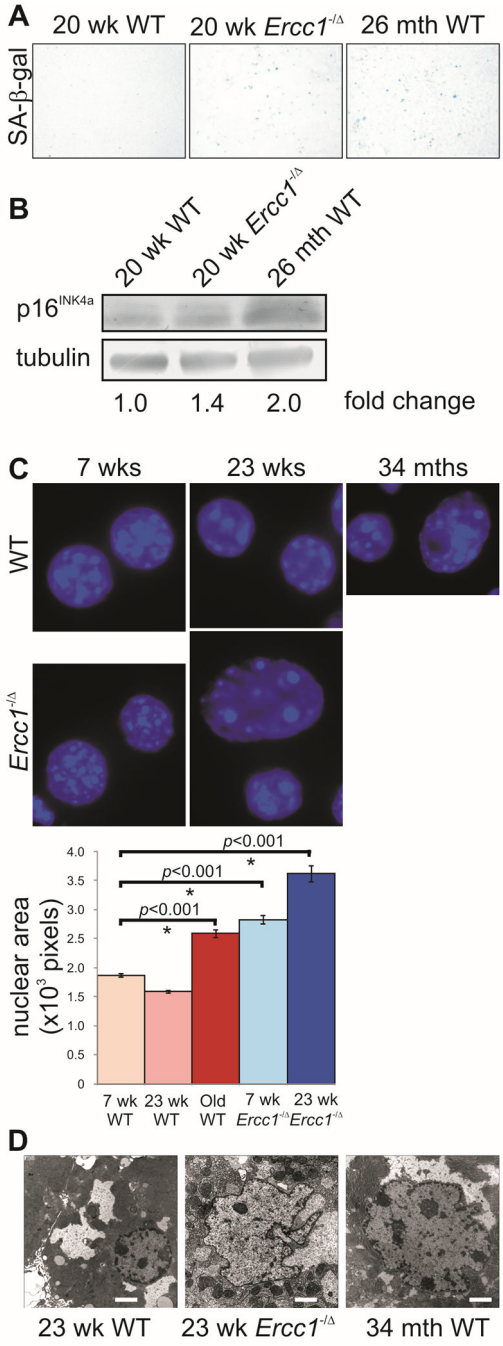

Figure 5. Premature senescence of *Ercc1*$^{-/\Delta}$ mouse liver

(A) Senescence-associated (SA) β-galactosidase histochemical stain on flash frozen liver sections.

(B) Immunoblot detection of the senescence marker p16^{INK4a} in liver lysates of a 20 week-old WT mouse and an *Ercc1*$^{-/\Delta}$ littermate, and a 26 month-old WT mouse. Tubulin was used as a loading control to calculate the fold-increase in p16 expression relative to adult WT mice.

(C) DAPI staining of hepatocyte nuclei illustrating increased nuclear size and heterogeneity in old WT (34 months) and adult *Ercc1*$^{-/\Delta}$ mouse liver (1000X). Quantification of nuclear size using Metamorph imaging software and images of DAPI-stained frozen liver sections.

Plotted are the average nuclear areas ± S.E.M. calculated from 10 random fields from 5 mice per group. The asterisks indicate significant differences.
(D) Transmission electron micrographs of representative hepatocyte nuclei (12,000X).

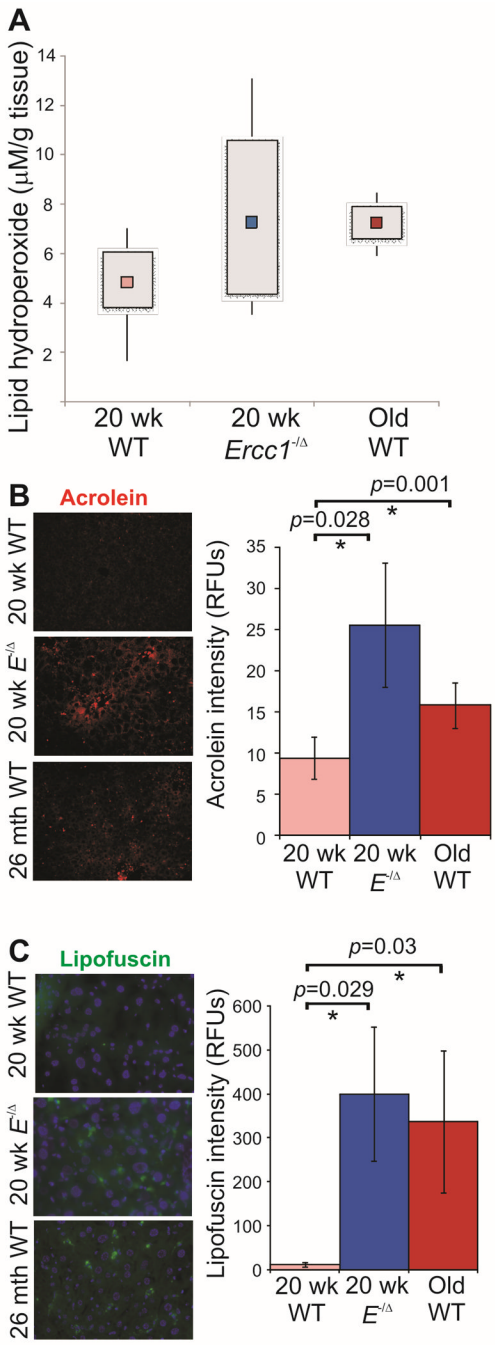

Figure 6. Increased oxidative damage in liver of old and progeroid mice

(A) Immunodetection of lipid hydroperoxides, a by-product of lipid peroxidation, in liver lysates from 20 wk-old WT and *Ercc1*$^{-/\Delta}$ littermate mice vs. old WT mice (26–34 months of age). The box plot represents the mean (in colored square), along with the 25th and 75th percentile for each group (n=5 mice). Average lipid hydroperoxide levels for groups were as follows: 20 wk WT (4.8μM/g liver), 20 wk *Ercc1*$^{-/\Delta}$ (7.3μM/g liver; p=0.12, one-tailed Student's t-test), and old WT (7.2μM/g liver).

(B) Immunofluorescence detection of acrolein, a by-product of lipid peroxidation. The staining intensity was quantified using AxioVision imaging software. Plotted are the

averages ± S.E.M. determined from analysis of 10 random fields of liver sections from 2 mice per group. Asterisks indicate significant differences.
(C) Representative images illustrating lipofuscin accumulation in 20 week-old WT and *Ercc1*$^{-/\Delta}$ mice and 26–34 month-old WT mouse liver. AxioVision software was used for quantification of 10 random fields measured from 5 mice per group. Plotted is the average fluorescence intensity for each group ± S.E.M. Asterisks indicate significant differences.

A

Suppression of oxidative metabolism					
code	Gene	5-wks FC	p	16-wks FC	p
1426059_at	Gckr	1.32	0.1353	-1.26	0.0066
1416090_at	Pdhb	-1.03	0.6851	-1.37	0.0001
1419146_a_at	Gck	-1.41	0.2856	-5.41	0.0000
1422577_at	Cs	-1.19	0.0171	-1.38	0.0006
1452206_at	Sucla2	-1.05	0.4352	-1.21	0.0004
1421258_a_at	Pklr	-1.32	0.3211	-2.03	0.0001
1443186_at	Pkm2	-1.52	0.2389	-2.87	0.0282
1455235_x_at	Ldh2	-16.70	0.3382	1.46	0.0328
1419737_a_at	Ldh1	1.12	0.0796	1.20	0.0056
Cell cycle arrest					
1424638_at	Cdkn1a	4.54	0.000	20.43	0.000
1440040_at	Cdk6	-1.13	0.718	1.96	0.019
1416868_at	Cdkn2c	1.25	0.082	1.79	0.000
1422439_a_at	Cdk4	1.28	0.046	1.66	0.001
1455287_at	Cdk6	1.16	0.239	1.54	0.001
1417649_at	Cdkn1c	-1.10	0.793	1.47	0.032
1449229_a_at	Cdkl2	1.05	0.743	1.27	0.007
1451741_a_at	Cdk7	1.44	0.025	1.27	0.013
1423067_at	Cdk5rap3	1.20	0.072	1.20	0.012
Response to DNA damage					
1421430_at	Rad51l1	2.23	0.041	2.43	0.013
1448497_at	Xpb	1.25	0.049	2.31	0.000
1449483_at	Polk	1.42	0.025	2.10	0.001
1417904_at	Dclre1a	2.31	0.001	2.02	0.000
1448520_at	Dclre1b	1.67	0.010	2.00	0.039
1424629_at	Brca1	1.26	0.204	1.98	0.000
1421731_a_at	Fen1	1.61	0.026	1.78	0.002
1443891_at	Rad51l3	-1.10	0.389	1.66	0.008
1416641_at	Lig1	1.60	0.008	1.57	0.001
1417572_at	Mpg	1.03	0.873	1.48	0.041
1417800_at	Parp2	1.57	0.011	1.37	0.027
1416602_a_at	Rad52	1.09	0.467	1.35	0.018
1433999_at	Slk	1.03	0.786	1.28	0.028
1460725_at	Xpa	1.03	0.863	1.28	0.022
1422624_at	Rev1l	-1.02	0.877	1.28	0.041
1416748_a_at	Mre11a	1.04	0.557	1.21	0.042
1437447_s_at	Ercc1	-4.47	0.000	-7.72	0.000

Upregulation of apoptosis					
code	Gene	5-wks FC	p	16-wks FC	p
1450971_at	Gadd45b	-1.80	0.198	3.17	0.012
1419004_s_at	Bcl2a1a	1.47	0.069	3.12	0.025
1437527_x_at	Mcl1	1.38	0.202	2.49	0.000
1449297_at	Casp12	-1.10	0.589	1.99	0.001
1416837_at	Bax	1.32	0.009	1.68	0.000
1415995_at	Casp6	1.42	0.001	1.36	0.017
1449491_at	Card10	-1.27	0.626	1.35	0.005
1450731_s_at	Tnfrsf21	-9.97	0.335	1.34	0.016
1416582_a_at	Bad	-1.08	0.571	1.27	0.047
Suppression of the GH/IGF1 axis and growth stimuli					
1418918_at	Igfbp1	2.36	0.125	4.05	0.008
1434413_at	Igf1	1.18	0.405	-1.22	0.024
1422826_at	Igfals	-1.11	0.657	-1.55	0.002
1452114_s_at	Igfbp5	-5.88	0.314	-1.79	0.017
1417962_s_at	Ghr	-1.28	0.001	-2.02	0.000
1417991_at	Dio1	-1.65	0.062	-14.51	0.000
1444166_at	Thrsp	-1.69	0.179	-1.75	0.007
1460420_a_at	Egfr	-1.31	0.320	-1.87	0.045
1451803_a_at	Vegfb	-2.15	0.079	-1.89	0.000
1419675_at	Ngfb	-1.22	0.107	-1.93	0.004
1450869_at	Fgf1	-1.52	0.001	-2.17	0.000
1438946_at	Pdgfra	-1.14	0.665	-2.19	0.003
Response to (oxidative) stress and detoxification					
1451695_a_at	Gpx4	1.05	0.762	1.55	0.000
1452135_at	Gpx6	-2.49	0.399	4.04	0.000
1456036_x_at	Gsto1	1.48	0.016	1.55	0.007
1416411_at	Gstm2	1.31	0.052	1.80	0.037
1416842_at	Gstm5	-1.58	0.400	1.56	0.001
1417883_at	Gstt2	1.52	0.046	1.31	0.005
1441931_x_at	Gss	-1.37	0.626	2.32	0.000
1428630_x_at	Haghl	1.31	0.379	1.70	0.000
1452592_at	Mgst2	1.66	0.318	3.86	0.045
1448300_at	Mgst3	-1.41	0.490	1.74	0.017
1437014_x_at	Prdx1	1.36	0.038	1.33	0.034
1450748_at	Smpd3	1.01	0.961	4.76	0.001
1416926_at	Trp53inp1	1.20	0.510	1.61	0.001
1416399_a_at	Hmox2	-1.09	0.308	1.23	0.001

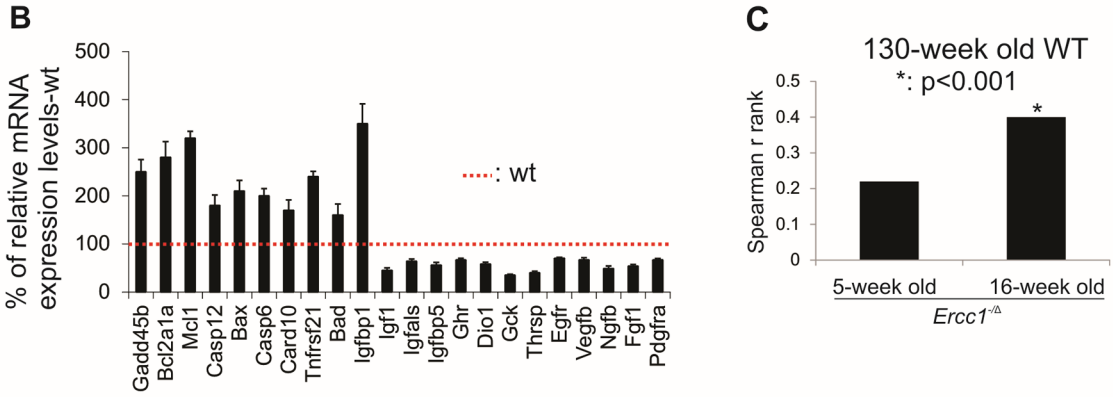

Figure 7. Age-associated transcriptional reprogramming in liver of *Ercc1*$^{-/\Delta}$ mice

(A) Significant gene expression changes (p<0.05, two tailed t-test) in the liver of 5- and 16-week old *Ercc1*$^{-/\Delta}$ mutant livers as compared to littermate control animals. Note the progressive dampening in the expression of genes involved in oxidative metabolism and the GH/IGF1 axis along with the upregulation in the expression of genes involved in cell cycle arrest, DNA damage responses, oxidative stress and detoxification (red color: up-regulated; green color: down-regulated, FC: fold change, wks: weeks).

(B) qPCR measuremtn of mRNA levels of a subset of genes identified to be differentially expressed in the liver of 16-week old Ercc1$^{-/\Delta}$ animals compared to wild-type littermates.

For each gene, expression levels in the mutant tissue are plotted relative to those of controls (red dotted line). Error bars indicate S.E.M. between replicates (n ≥ 4).
(C) Spearman's r correlation reflecting transcriptome similarities between the 5 or 16 week-old *Ercc1*$^{-/\Delta}$ and the 130 week-old mouse livers where −1.0 is a perfect negative (inverse) correlation, 0.0 is no correlation, and 1.0 is a perfect positive correlation.